# CHAPTER V
# RESULTS AND DISCUSSION

Since this work was continued from previous work (Chaikasetpaiboon *et al.*, 2002), sensitivity analysis was initially performed to study the parametrical effects on theoretical breakthrough curves in order to investigate and develop the existing mathematical model.

Furthermore, the adsorption isotherm of water on each adsorbent was determined on the experimental apparatus. The study of water breakthrough behaviors for the multi-layer adsorber at various humidity levels and contact times are discussed and reported. Finally, the isotherm equations and the theoretical breakthrough curves predicted from the mathematical model are proposed in this chapter.

## 5.1 Sensitivity Analysis of the Existing Model

To improve the mathematical model and to study the parametrical effects on the breakthrough curves, a parameter sensitivity analysis was performed. From the existing model:

$$-\mathbf{D}_{\mathbf{L,eff}}\frac{\partial^2 c}{\partial z^2}+\mathbf{v}\frac{\partial c}{\partial z}+\frac{\partial c}{\partial t}+\left(\frac{1-\boldsymbol{\varepsilon}_{\mathbf{eff}}}{\boldsymbol{\varepsilon}_{\mathbf{eff}}}\right)\frac{\partial \overline{q}_{\mathbf{eff}}}{\partial t}=0 \qquad (5.1)$$

three parameters were analyzed: effective axial dispersion coefficient ($D_{L,eff}$), interstitial velocity (v) and effective bed voidage ($\varepsilon_{eff}$). The sensitivity of those parameters are revealed in Figures 5.1, 5.2 and 5.3. It was observed that the interstitial velocity (v) and bed voidage ($\varepsilon$) were more sensitive to the theoretical breakthrough curves than the axial dispersion coefficient ($D_L$) because when the interstitial velocity and/or the bed voidage decreased, the breakthrough times were highly increased. Therefore, the existing mathematical model might be modified in terms of the interstitial velocity by taking into account that the interstitial velocity along the bed was not constant, and the properties of each adsorbent such as the

adsorption isotherm, bed voidage and dispersion coefficient were specifically used in the mathematical model.

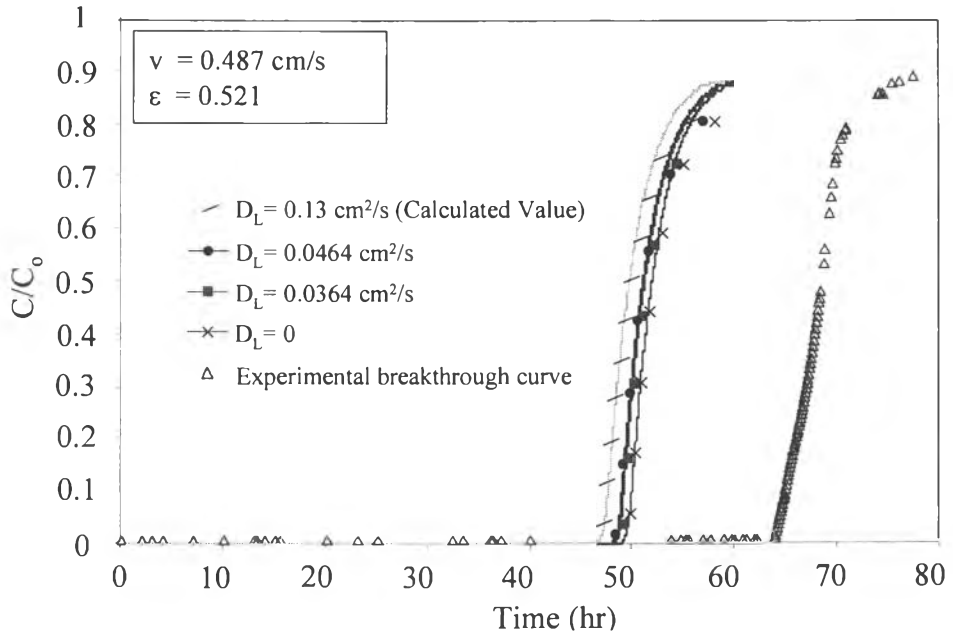


**Figure 5.1** Influence of effective axial dispersion coefficient ($D_{L,eff}$) on the theoretical breakthrough curve.

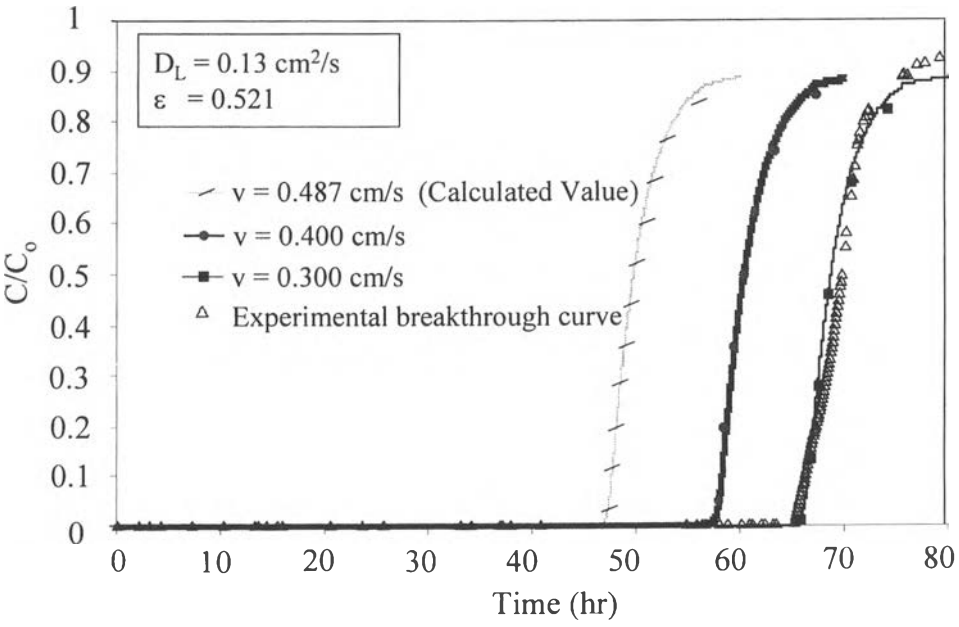


**Figure 5.2** Influence of interstitial velocity (v) on the theoretical breakthrough curve.

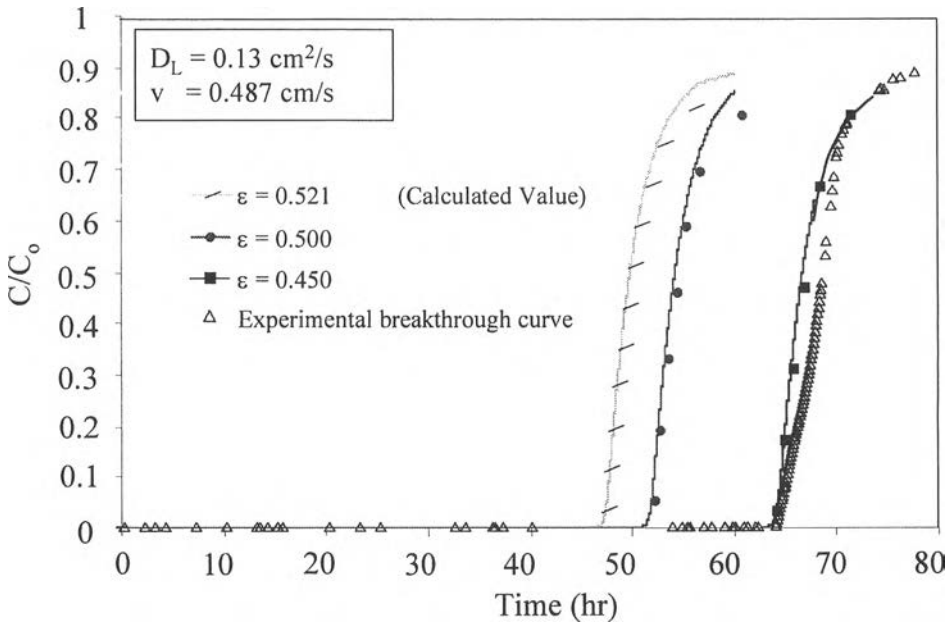


**Figure 5.3** Influence of effective bed voidage ($\varepsilon_{eff}$) on the theoretical breakthrough curve.

## 5.2 Adsorption Isotherm Data

### 5.2.1 Silica Gel

The equilibrium water adsorption capacity at 25°C and 1 atm for silica gel is shown in Figure 5.4. It was observed that silica gel adsorbed water vapor well at high inlet water concentration in the gas phase because at a low surface coverage, the water molecule is bound to the silanol group "oxygen down":

$$\equiv Si{-}OH \cdots OH_2$$

but at higher coverages, hydrogen bonding within clusters of water becomes predominant , with a bond strength or heat of adsorption approaching the liquefaction energy of water (Yang, 1987).

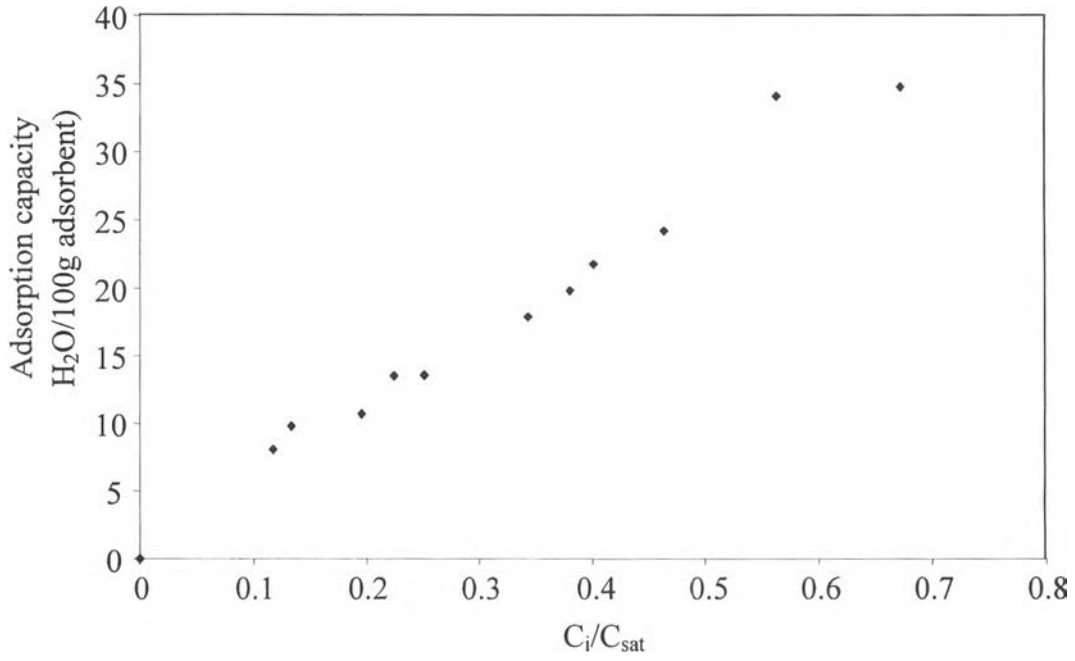


**Figure 5.4** Experimental data for modeling equilibrium adsorption isotherm of water on silica gel at 25 °C, and 1 atm.

5.2.2 4A Molecular Sieve with the Pellet Size of 1/8" and 1/16"

The experimental adsorption isotherms of 4A molecular sieve with the pellet size of 1/8" and 1/16"were analogous to Type II and Type IV Brunauer isotherms, respectively, and these might indicate that in the porous adsorbent there is a continuous progression from monolayer to multilayer when increasing loading and, then, to capillary condensation (Ruthven, 1984). Moreover, this may indicate that more water molecules were adsorbed even after the first layer was filled. This occurred because the saturation vapor pressure in a small pore was reduced, in accordance with the Kelvin equation by the effect of surface tension. The adsorption isotherms of 4A molecular sieve 1/8" and 1/16" are shown in Figures 5.5 and 5.6, respectively.

In the capillary condensation region the isotherm generally shows hysteresis, meaning the apparent equilibrium pressures observed in adsorption and desorption experiments are different. The relationship between pressure and adsorbed phase concentration along the adsorption branch of the isotherm will be governed by a multilayer isotherm such as the BET equation (although the BET

equation itself is not applied in this region as frequently as in the relative pressure range of less than about 0.35 (Ruthven, 1984)).

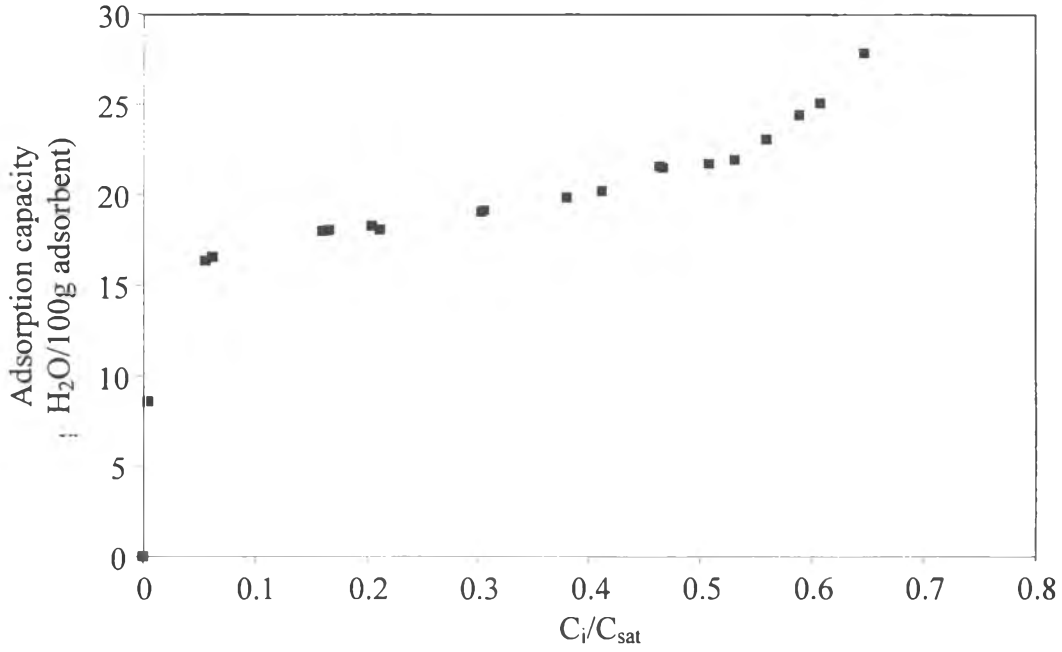


**Figure 5.5** Experimental data for modeling equilibrium adsorption isotherm of water on 4A molecular sieve 1/8" at 25 °C, and 1 atm.

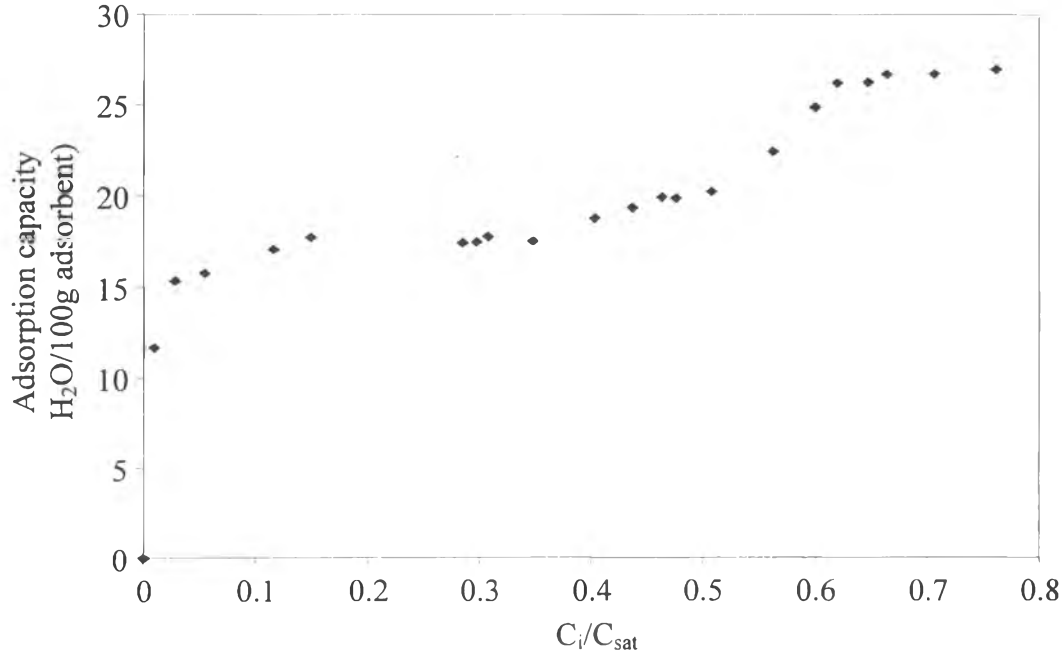


**Figure 5.6** Experimental data for modeling equilibrium adsorption isotherm of water on 4A molecular sieve 1/16" at 25 °C, and 1 atm.

## 5.3 Experimental Breakthrough Curves

The response of a water free adsorber to a step change in water concentration at the column inlet was considered in order to study the dynamics of a fixed-bed adsorber. The experimentally obtained breakthrough curves of water carried out at various operating conditions are plotted in Figures 5.7 to 5.11 for water breakthrough from the multi-layer adsorber. In these figures, the dimensionless concentration is plotted against time. To study the effects of water concentrations at the inlet gas on the breakthrough behaviors, the experiments were carried out with varied feed concentrations of 7, 30, and 50%RH. As observed from the Figures 5.7 and 5.8, the breakthrough times operating at the inlet gas concentrations of 30 and 50%RH are about 107 and 73 hours for the constant contact time of 34 seconds and about 52 and 34 hours for the constant contact time of 17 seconds, respectively.

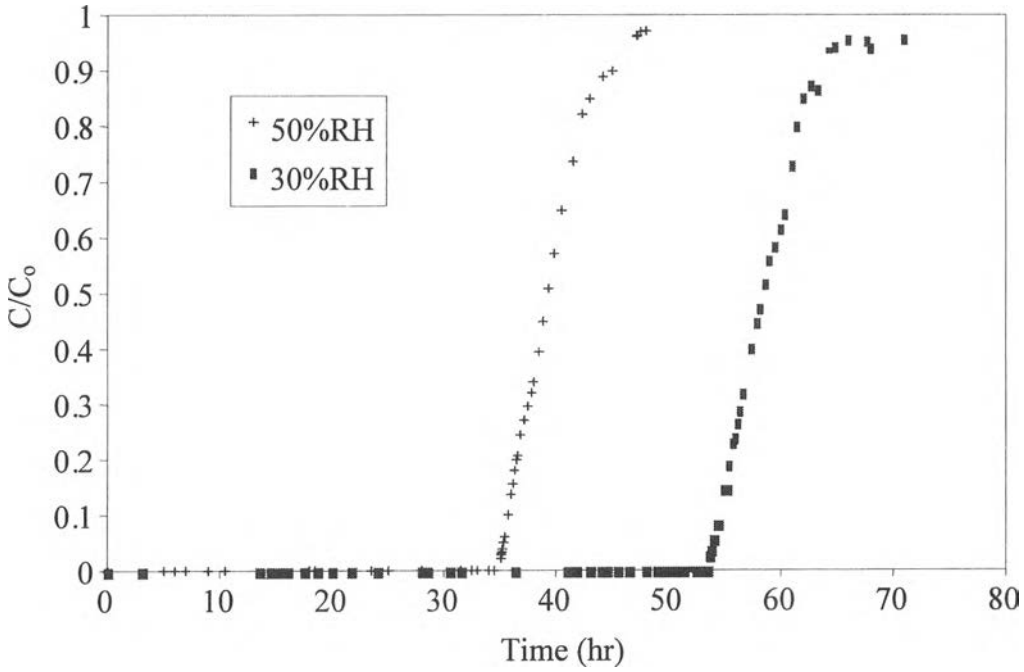


**Figure 5.7** Effects of water contents in natural gas feed on breakthrough curves at the constant contact time of 17 sec.

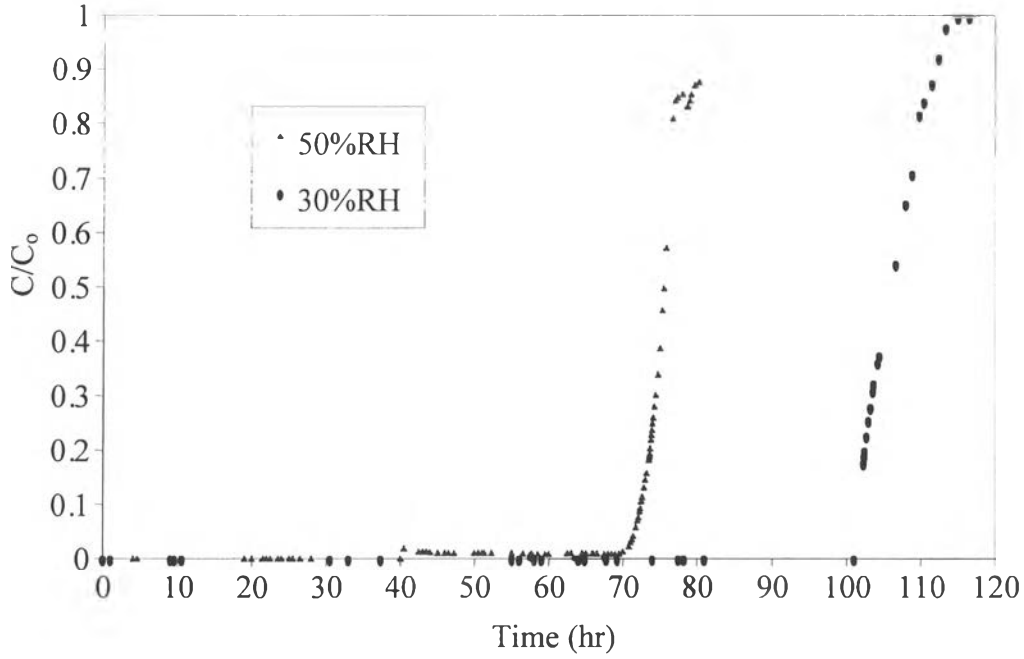


**Figure 5.8** Effects of water contents in natural gas feed on breakthrough curves at the constant contact time of 34 sec.

Additionally, the dynamic adsorption at low water concentration in the natural gas feed was considered. The experimental breakthrough data during dynamic adsorption carried out with 7%RH and the constant contact time of 34 seconds is illustrated in Figure 5.9. As these operating conditions, the amount of time consumed at the point where the water concentration of the effluent began to appear was about 408 hours.

According to Figures 5.10 and 5.11, the higher feed flow rate (lower contact time) results in the earlier breakthrough time. This is due to the fast saturation of adsorbents with water as a greater amount of water flows through the bed in a shorter time.

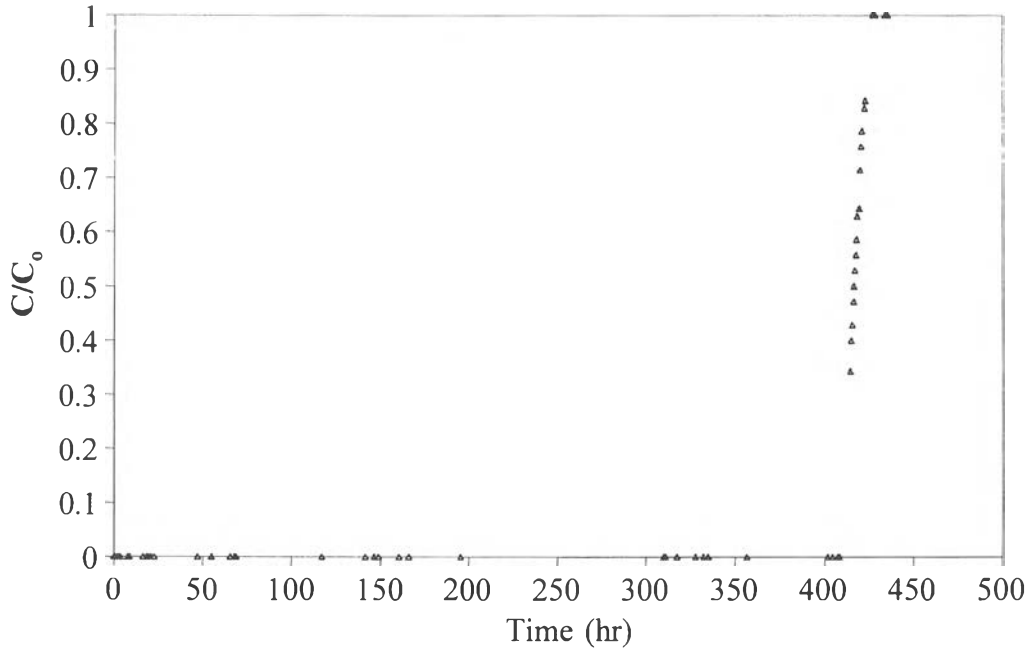


**Figure 5.9** Experimental breakthrough data with the inlet water concentration of 7%RH at the constant contact time of 34 sec.

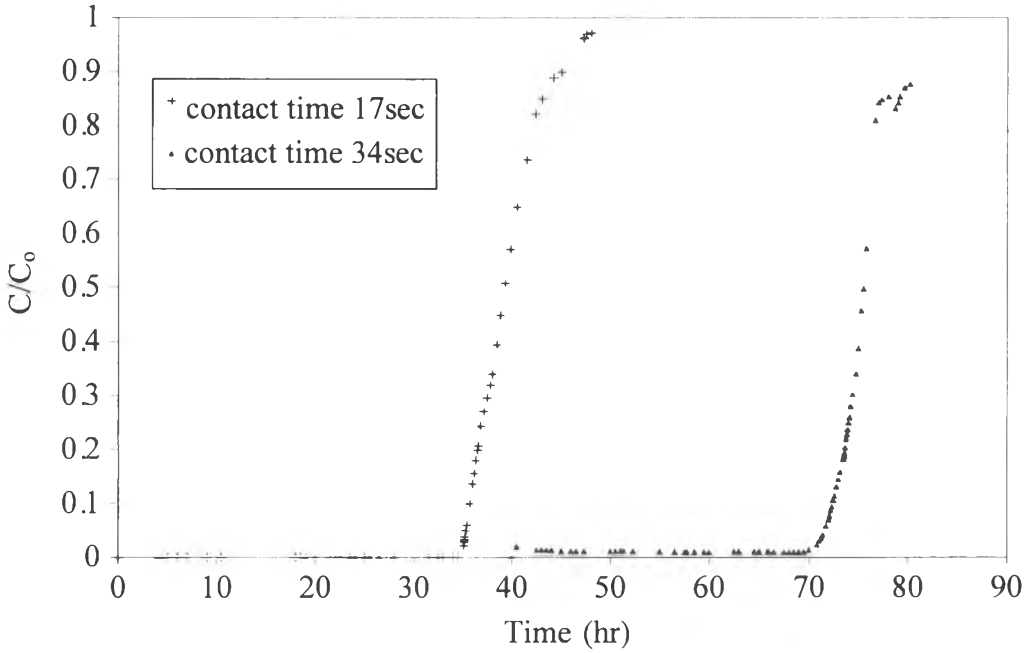


**Figure 5.10** Effects of contact times (or feed flow rates) on breakthrough curves with the inlet humidity level of 50%RH.

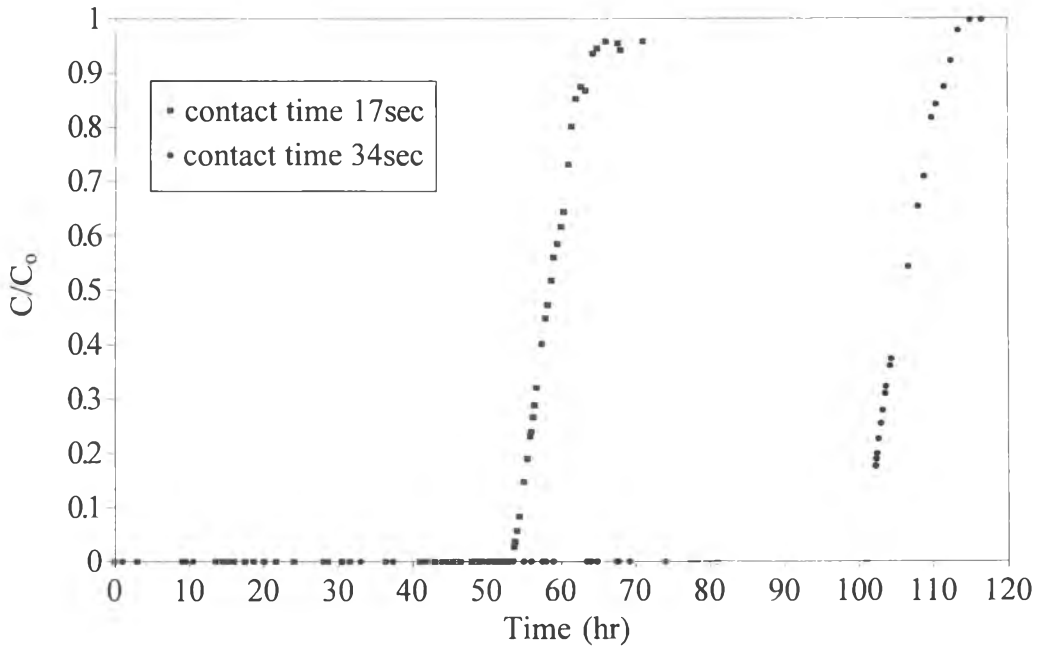


**Figure 5.11** Effects of contact times (or feed flow rates) on breakthrough curves with the inlet humidity level of 30%RH.

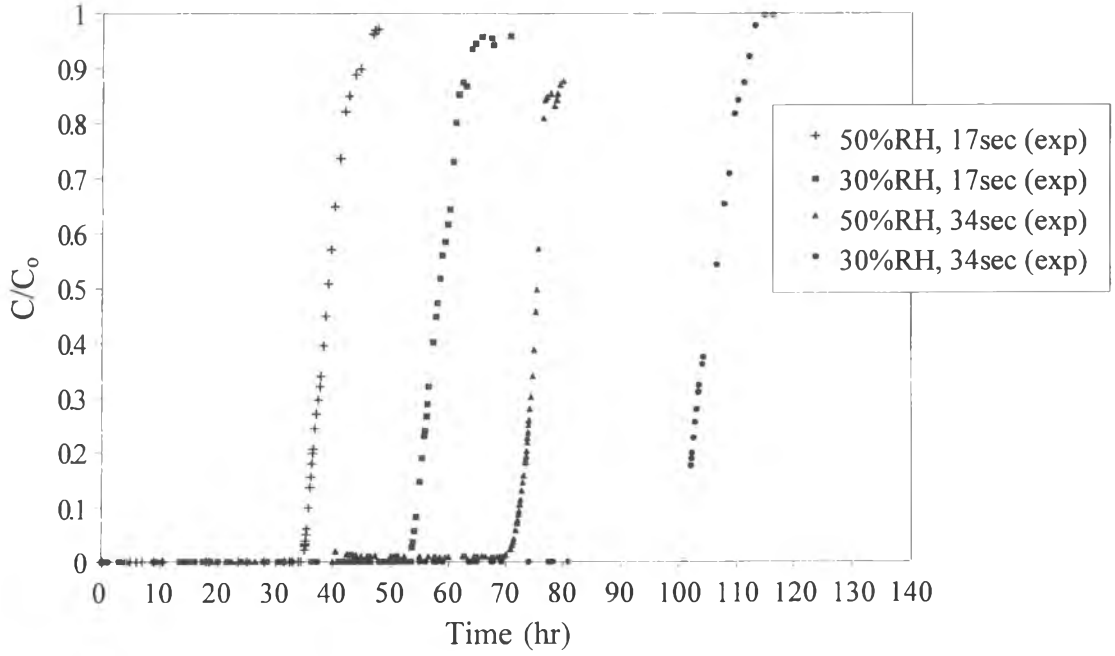


**Figure 5.12** The experimental breakthrough data of various operating conditions.

## 5.4 Mathematical Models for the Adsorption on a Multi-layer Adsorber

### 5.4.1 Equilibrium Adsorption Isotherm Models

#### *5.4.1.1 Silica Gel*

The adsorption isotherm of silica gel is shown in Figure 5.13. The equilibrium adsorption models, which are Linear and Freundlich models, were applied to give a good correspondence with the experimental data points taken from part 5.2.1.

The equilibrium adsorption constants of Linear and Freundlich models for silica gel are presented in Table 5.1. The constants were obtained by using a regression technique in the Sigma Plot program.

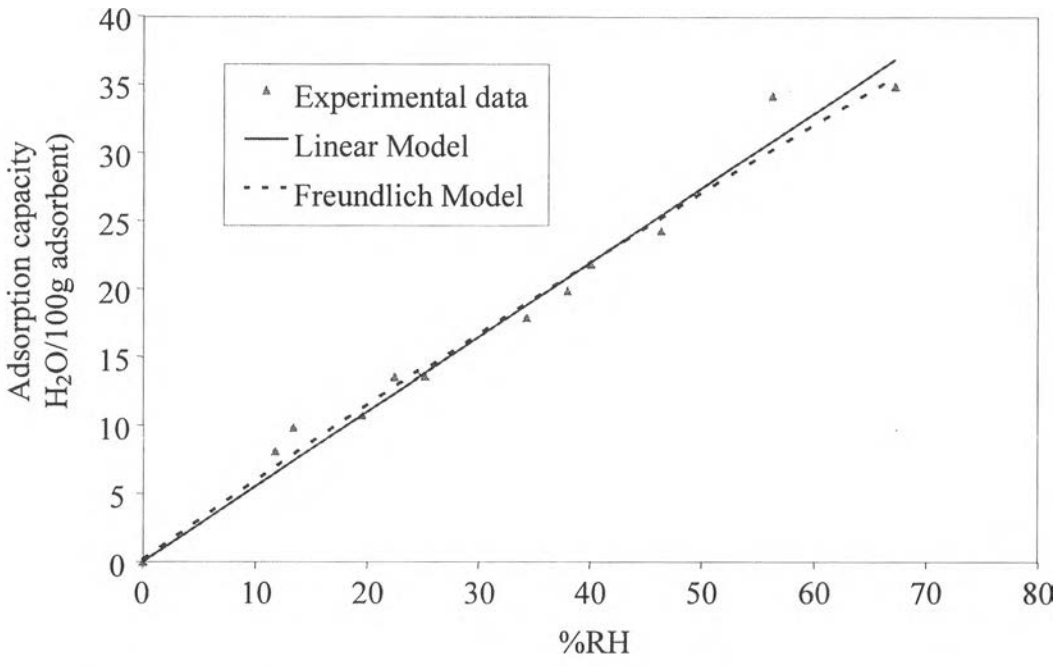


**Figure 5.13** Equilibrium adsorption models for silica gel.

**Table 5.1** Constants in adsorption isotherm models for silica gel

| Model | Equation ‡ | Constant |
|---|---|---|
| Linear | $q = a_1 c$ | $a_1 = 54.7460$<br>$R^2 = 0.9762$ |
| Freundlich | $q = a_2 c^{n_1}$ | $a_2 = 52.0232$<br>$n_1 = 0.9345$<br>$R^2 = 0.9704$ |

‡ concentration in mol/l

*5.4.1.2 4A Molecular Sieve 1/8"*

From the experimental data shown in Figure 5.5, the equilibrium adsorption isotherm of 4A molecular sieve 1/8" was divided into two regions as illustrated in Figure 5.14. The first region is a range of humidity level from 0%RH to 22 %RH, whereas the second region is above 22%RH. The Langmuir model was applied to make a good fit with the experimental data points in the first region, whereas an exponential model demonstrated a good representative of the experimental data points in the second region.

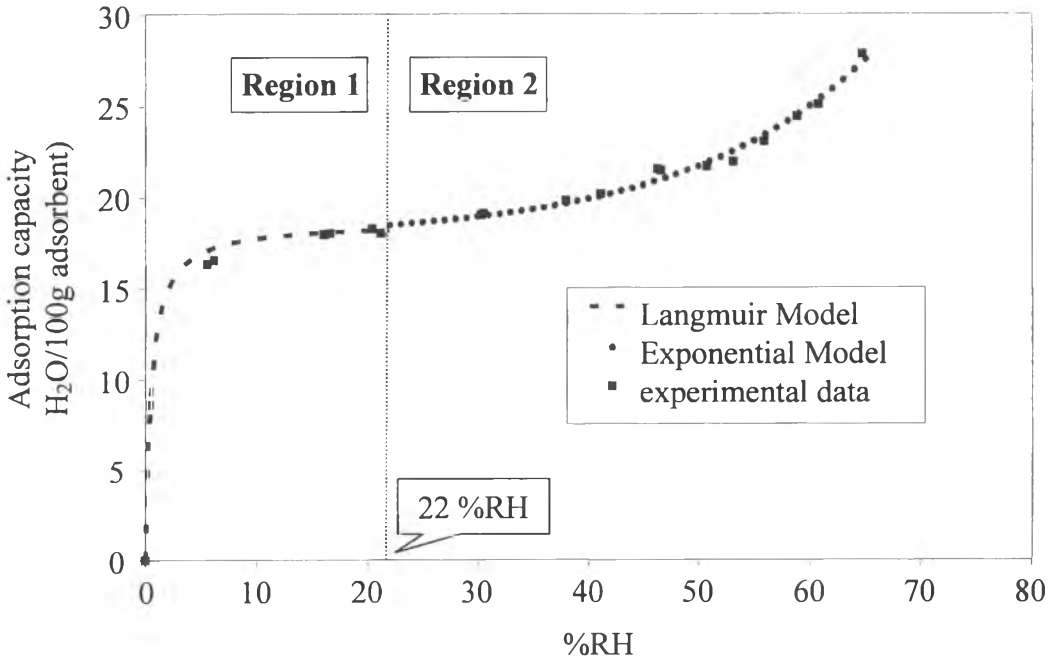


**Figure 5.14** Equilibrium adsorption models for 4A molecular sieve 1/8".

The constants in Langmuir and exponential models for the 4A molecular sieve 1/8" are presented in Table 5.2. The constants were obtained by using a regression technique in the Sigma Plot program.

**Table 5.2** Constants in adsorption isotherm equations for 4A molecular sieve 1/8"

| Region | Model | Equation ‡ | Constant |
|---|---|---|---|
| 1 | Langmuir | $q = \frac{a_3 c}{1 + b_1 c}$ | $a_1$ = 3787.25<br>$b_1$ = 203.54<br>$R^2$ = 0.9933 |
| 2 | Exponential | $q = y_1 + a_3 e^{m_1 c}$ | $y_1$ = 17.7844<br>$a_2$ = 0.1840<br>$m_1$ = 6.1116<br>$R^2$ = 0.9881 |

‡ concentration in mol/l

*5.4.1.3 4A Molecular Sieve 1/16"*

From part 5.2.2, the equilibrium adsorption isotherm of 4A molecular sieve 1/16" was separated into three regions. The first region is in a range of humidity level from 0%RH to 32 %RH, the second region is in a range of humidity level between 32%RH to 62%RH, whereas the third region is above 62%RH as shown in Figure 5.15. The Langmuir and exponential model were employed to make a good fit with the experimental data points in the first and the second regions, respectively, whereas the linear and Freundlich models demonstrated a good representative of the experimental data points in the third region. The constants in all models for 4A molecular sieve 1/16" are presented in Table 5.3. The constants were obtained by using a regression technique in the Sigma Plot program.

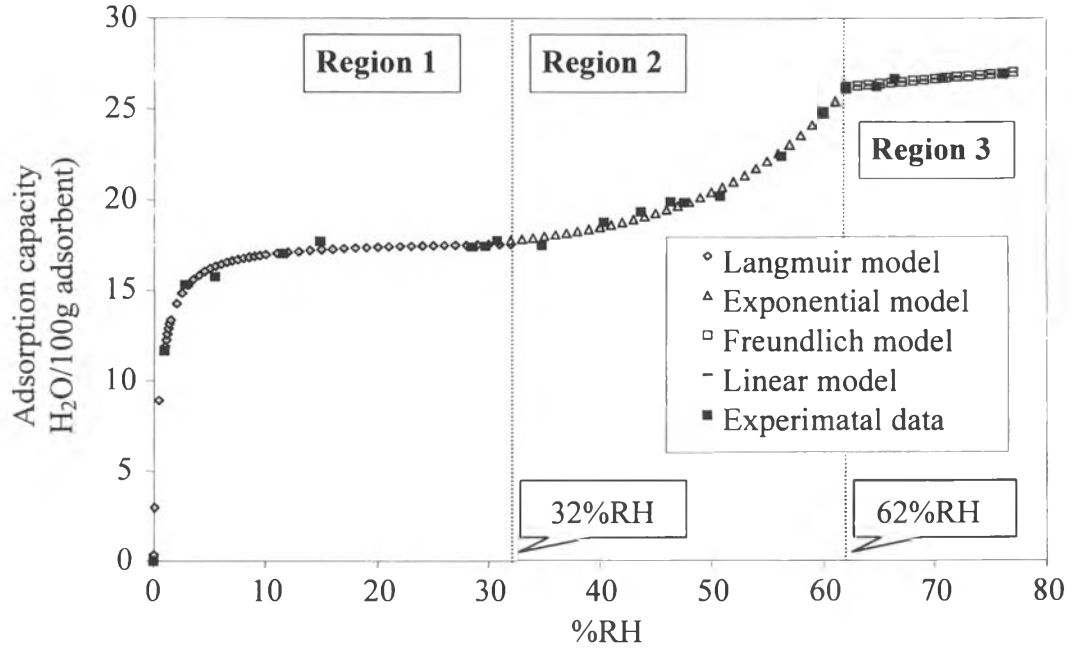


**Figure 5.15** Equilibrium adsorption models for 4A molecular sieve 1/16".

**Table 5.3** Constants in adsorption isotherm equations for 4A molecular sieve 1/16"

| Region | Model | Equation‡ | Constant |
|---|---|---|---|
| 1 | Langmuir | $q = \frac{a_4 c}{1 + b_2 c}$ | $a_4$ = 3568.02<br>$b_2$ = 200.23<br>$R^2$ = 0.9976 |
| 2 | Exponential | $q = y_2 + a_5 e^{m_2 c}$ | $y_2$ = 16.9832<br>$a_5$ = 0.0562<br>$m_2$ = 8.2131<br>$R^2$ = 0.9881 |
| 3 | Linear | $q = y_3 + a_6 c$ | $y_3$ = 22.8552<br>$a_6$ = 5.3972<br>$R^2$ = 0.8406 |
| | Freundlich | $q = a_7 c^{n_2}$ | $a_7$ = 28.0116<br>$n_2$ = 0.1405<br>$R^2$ = 0.8482 |

‡ concentration in mol/l

5.4.2 Theoretical Breakthrough Curves

After the sensitivity analysis was performed to study the parametrical effects on the theoretical breakthrough curves, the mathematical model was developed to predict the experimental breakthrough time under varying operating conditions. The mass transfer rate described by linear driving force (LDF) model was involved in the overall model. The mathematical model for water breakthrough curve is based on the assumptions of an axially dispersed plug flow, isothermal system, constant fluid velocity, and no pressure drop. The physical properties and the equilibrium adsorption isotherm constructed for each adsorbent were utilized in the model. The parameters of each adsorbent were presented in Table 4.1.

The FORTRAN computer language was programmed to solve the mathematical model for predicting the experimental breakthrough profile at various operating conditions. The program details are reported in Appendix D.

*5.4.2.1 Effect of Overall Mass Transfer Coefficient (k) on Theoretical Breakthrough Curves*

In order to obtain the best agreement between the experimental and mathematical breakthrough curves, the overall mass transfer coefficient (k) should be adjusted. The increase in k value means the increase in the mass transfer rate. If the mass transfer rate is increased, the mass transfer zone will be depressed. As a result, the steeper curve is generated.

From the theoretical breakthrough curves in Figure 5.16, when k was about $8.5 \times 10^{-5}$ $s^{-1}$, the theoretical breakthrough pattern is similar to the experimental one. In fact, the different operating conditions should have the different k values; however, the pattern of the experimental breakthrough curve for each case was not much different. Therefore, the k value of about $8.5 \times 10^{-5}$ $s^{-1}$ was reasonably suggested for all experimental conditions.

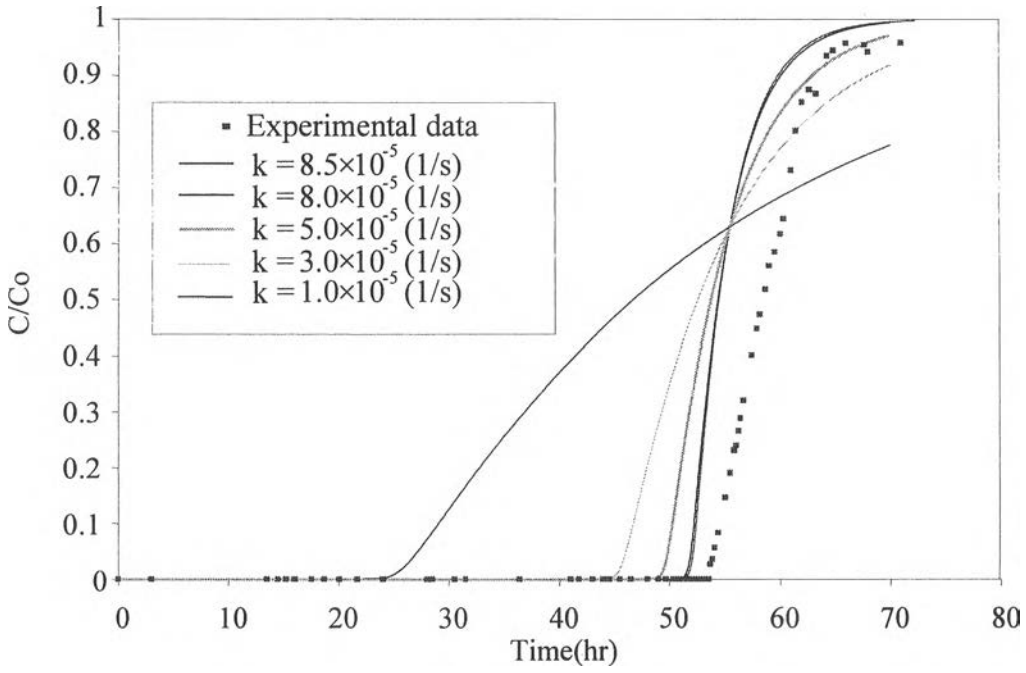


**Figure 5.16** Influence of mass transfer coefficient (k) on theoretical breakthrough curves at the contact time of 17 sec and the feed humidity of 30%RH.

*5.4.2.2 Comparison of Experimental and Theoretical Breakthrough Curves*

The predicted breakthrough profiles for water adsorption on the multi-layer adsorber under the various operating conditions were depicted in Figures 5.17 and 5.18. The mathematical model was observed to be in good agreement with the experimental data under identical conditions. In each case, the difference between the experimental and theoretical breakthrough time is about 3 to 5% as illustrated in Table 5.4. These deviations might be due to the instrumental errors.

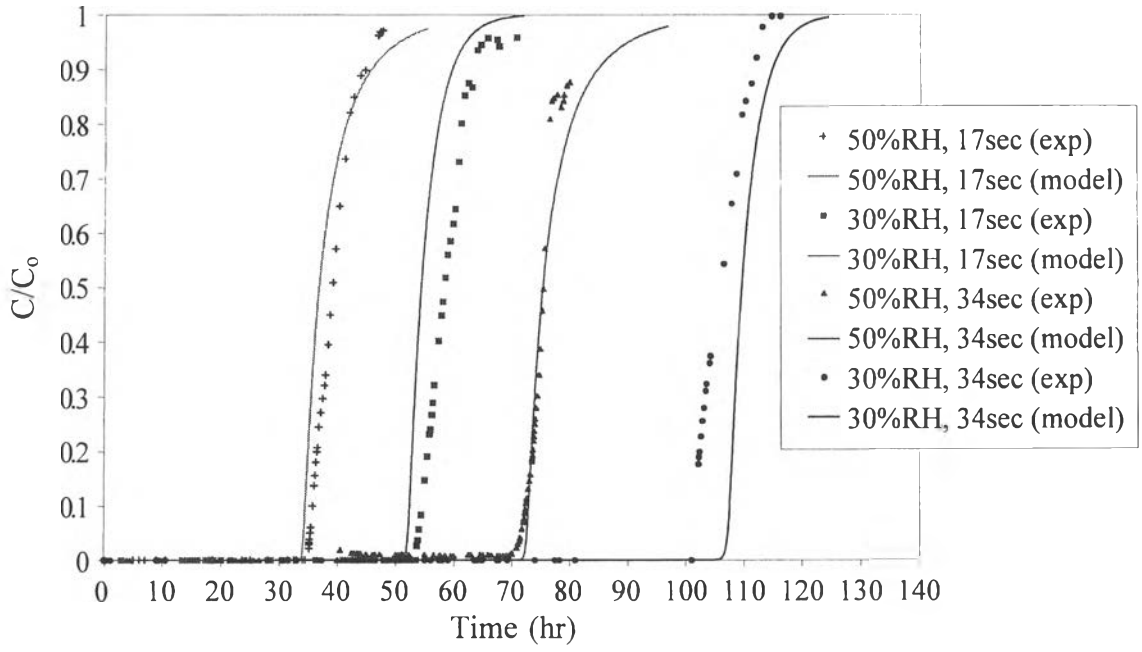


**Figure 5.17** Comparison of experimental and mathematical breakthrough curves.

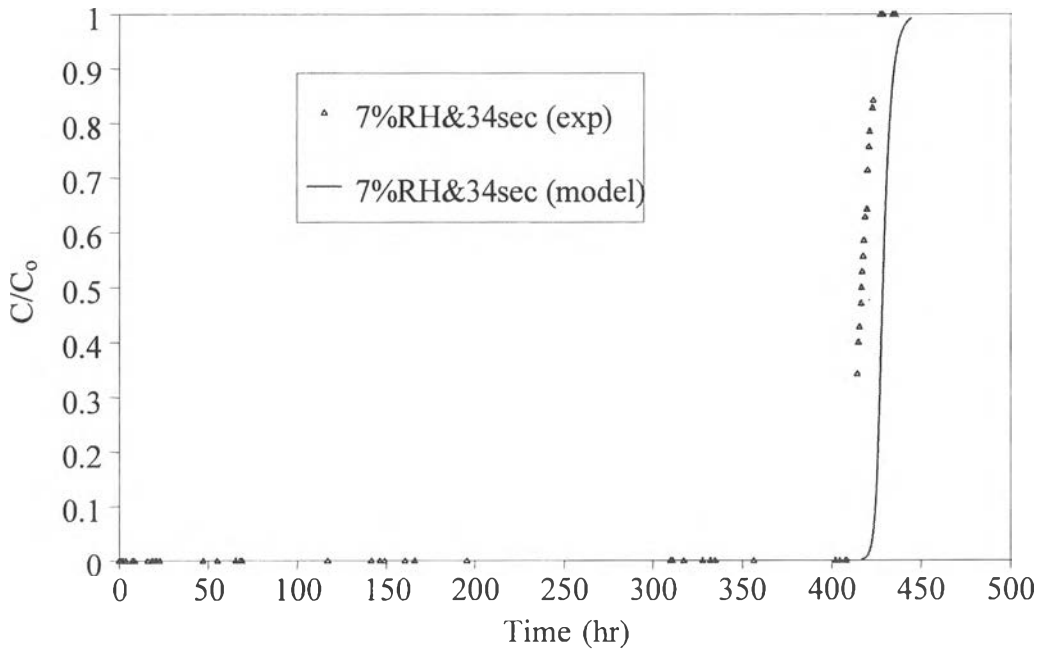


**Figure 5.18** Comparison between experimental and mathematical breakthrough curves at the contact time of 34 sec and the feed humidity of 7%RH.

**Table 5.4** Comparison between the experimental and theoretical breakthrough time

| Condition | | Breakthrough Time (hours) | | |
|---|---|---|---|---|
| Concentration (%RH) | Contact time (seconds) | Experiment | Model | Error (%) |
| 7 | 34 | 408.5 | 420.5 | 2.94 |
| 30 | 34 | 101.5 | 106.7 | 5.12 |
| 50 | 34 | 70.0 | 73.0 | 4.29 |
| 30 | 17 | 53.7 | 52.0 | 3.17 |
| 50 | 17 | 35.1 | 34.0 | 3.13 |

*5.4.2.3 Characteristic of Interstitial Velocity Profile in A Multi-layer Adsorber*

The variation of the interstitial velocity ($v_i$) with time depends on the bed voidage ($\varepsilon_t$) and the amount of water adsorbed on the adsorbents. Since three different types of the commercial adsorbents were packed in the adsorber, the different bed void fractions exist in the column. As a result, the interstitial velocity was different in each layer of packed adsorbent. According to Figure 5.19, the interstitial velocity in silica gel layer is the lowest because of the highest bed void fraction. Moreover, the decrease in the interstitial velocity was due to the adsorption of water over the adsorbent. Since there was the small amount of water content in the natural gas, the decrease in the interstitial velocity by the adsorption was very low. Figure 5.20 compares between the theoretical breakthrough time obtained from the mathematical model with the assumption of inconstant fluid velocity and that with the assumption of constant fluid velocity. It was observed that the breakthrough curves were not different. Therefore, the variation of the interstitial velocity due to the adsorption could have been assumed to be constant.

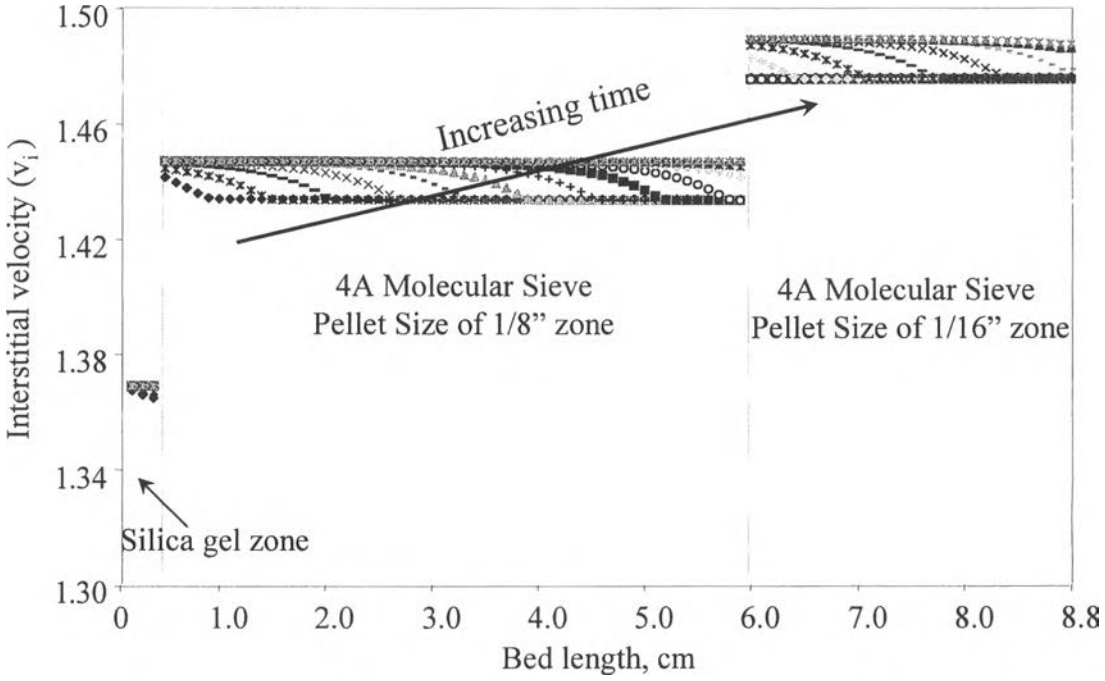


**Figure 5.19** Variation of interstitial velocity with operating time at the contact time of 17 sec, and the feed humidity of 30%RH.

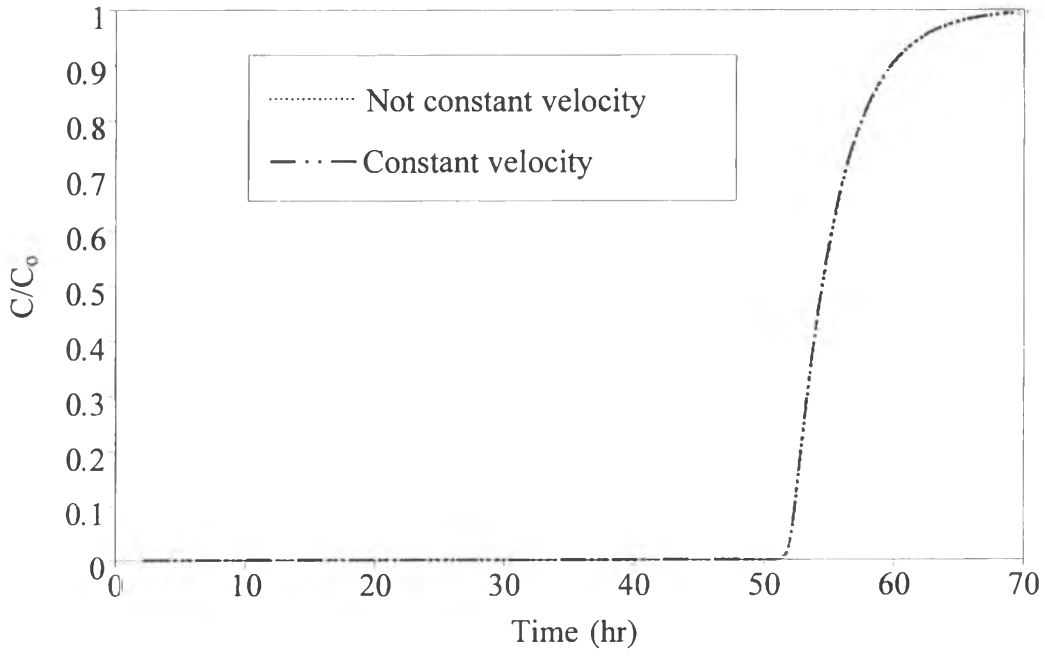


**Figure 5.20** Comparison of the theoretical breakthrough curve between the assumptions of inconstant fluid velocity and constant fluid velocity.